Hydrodeoxygenation of Phenol to Benzene and Cyclohexane on Rh(111) and Rh(211) Surfaces: Insights from Density Functional Theory

Garcia-Pintos, Delfina; Voss, Johannes; Jensen, Anker Degn; Studt, Felix

Published in:
The Journal of Physical Chemistry Part C: Nanomaterials, Interfaces and Hard Matter

Link to article, DOI:
10.1021/acs.jpcc.6b02970

Publication date:
2016

Document Version
Publisher's PDF, also known as Version of record

THE JOURNAL OF PHYSICAL CHEMISTRY C

Article

pubs.acs.org/JPCC

Hydrodeoxygenation of Phenol to Benzene and Cyclohexane on Rh(111) and Rh(211) Surfaces: Insights from Density Functional Theory

Delfina Garcia-Pintos,[†,⊥] Johannes Voss,[†,⊥] Anker D. Jensen,[‡] and Felix Studt*[,†,⊥,§,∥]

[†]SUNCAT Center for Interface Science and Catalysis, SLAC National Accelerator Laboratory, 2575 Sand Hill Road, Menlo Park, California 94025, United States

[⊥]Department of Chemical Engineering, Stanford University, Stanford, California 94305, United States

[‡]Department of Chemical and Biochemical Engineering, Technical University of Denmark, Søltofts Plads, Building 229, DK-2800 Lyngby, Denmark

[§]Institute of Catalysis Research and Technology, Karlsruhe Institute of Technology, Hermann-von-Helmholtz Platz 1, 76344 Eggenstein-Leopoldshafen, Germany

[∥]Institute for Chemical Technology and Polymer Chemistry, Karlsruhe Institute of Technology, Engesserstr. 18, 76131 Karlsruhe, Germany

Supporting Information

ABSTRACT: Herein we describe the C−O cleavage of phenol and cyclohexanol over Rh(111) and Rh(211) surfaces using density functional theory calculations. Our analysis is complemented by a microkinetic model of the reactions, which indicates that the C−O bond cleavage of cyclohexanol is easier than that of phenol and that Rh(211) is more active than Rh(111) for both reactions. This indicates that phenol will react mainly following a pathway of initial hydrogenation to cyclohexanol followed by hydrodeoxygenation to cyclohexane. We show that there is a general relationship between the transition state and the final state of both C−O cleavage reactions, and that this relationship is the same for Rh(111) and Rh(211).

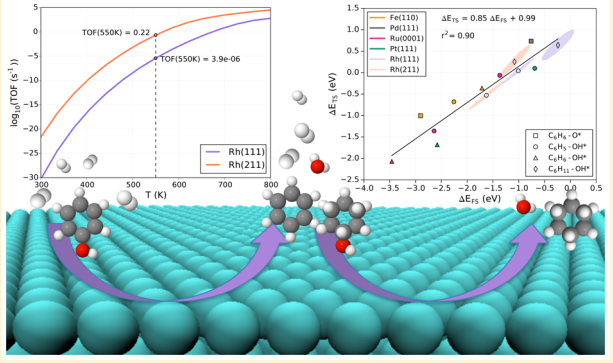

1. INTRODUCTION

Modern society relies on oil as the primary feedstock for the production of transportation fuels. Not only are the reserves limited and are getting ever more expensive to exploit,[1,2] the utilization of oil has also very negative environmental effects as, e.g., expressed by emissions of carbon dioxide. To divert the production of transportation fuels to renewable resources is therefore gaining increasing attention. In this concept, lignocellulosic biomass is particularly interesting as it represents the nonedible part of biomass and therefore does not compete with societies food-supply.

There are several avenues that are currently being investigated for the production of fuels from lignocellulosic sources. Among them fast pyrolysis followed by upgrading through hydrodeoxygenation (HDO) is particularly promising.[3−5] The bio-oil that is derived from fast pyrolysis is characterized by high viscosity and a high oxygen content. It is a multicomponent mixture containing water and several hundreds of compounds with a wide variety of functional groups such as acids, aldehydes, ketones, phenolics, and alcohols.[6] Among these, phenols are particularly abundant and bio-oil often contains up to 30 wt % of phenolic compounds such as phenols, guaiacols, and syringols.[7] The most desired products of HDO of these phenolic compounds are benzene and its derivatives since the consumption of costly hydrogen is much reduced when unsaturated molecules are produced.

HDO of phenolic compounds has been studied experimentally mainly on supported noble and non-noble metals, as well as sulfided Co/Ni−Mo catalysts, using phenol, guaiacol, and diverse types of substituted phenol.[3,6−21] Few studies addressed HDO from a theoretical point of view, usually using density functional theory (DFT) calculations.[22−27] Due to the complexity of phenols contained in bio-oil, model compounds such as phenol and guaiacol are usually considered for studies of catalytic hydrodeoxygenation. Guaiacol HDO has been studied over Ru(0001) and Pt(111) surfaces,[22−24] Fe−Ni surfaces have been evaluated for the adsorption of furfural,[25] and the dissociation of phenol to phenoxy has been investigated on Pt,[26] Rh,[26] Pd,[27] and Fe[27] surfaces.

Received: March 22, 2016
Revised: July 22, 2016
Published: July 22, 2016

DOI: 10.1021/acs.jpcc.6b02970
J. Phys. Chem. C 2016, 120, 18529−18537

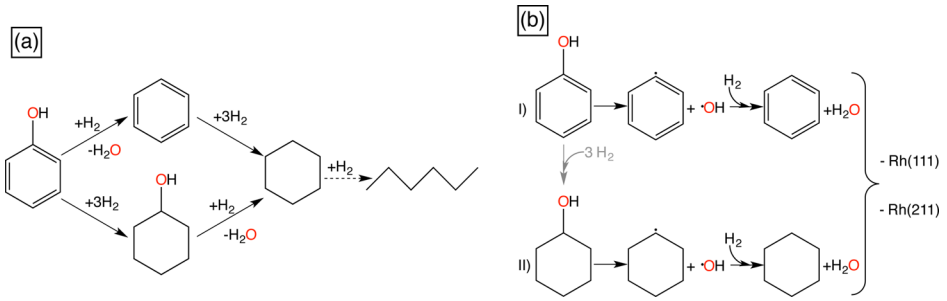

Figure 1. (a) Reaction network showing possible routes for phenol hydrodeoxygenation. (b) Reaction paths showing phenol hydrodeoxygenation through direct deoxygenation (DDO) with aromatic C−O bond cleavage (path I) and hydrodeoxygenation of cyclohexanol (path II), which have been studied on Rh(111) and Rh(211) in this work.

Herein, we study the conversion of phenol to benzene and cyclohexane on different facets of rhodium catalysts using DFT calculations. We chose rhodium as the starting point in our investigations, taking into account that its catalytic properties are often comparable to those of nonprecious metals like, e.g., Ni. We investigate both, the direct deoxygenation of phenol yielding benzene via aromatic C−O bond scission and the HDO of cyclohexanol (derived from phenol) yielding cyclohexane. We address the structure sensitivity of these reactions employing Rh(111) and Rh(211) surfaces to mimic the least and most reactive facets of Rh particles. Using our DFT results as an input we develop a microkinetic model of these reactions and show how activity can be improved using a degree of rate control analysis.

2. METHODS

2.1. Density Functional Theory Calculations. Plane-wave periodic density functional theory (DFT) calculations were performed using the Vienna Ab-initio Simulation Package (VASP)[28,29] and the Atomic Simulation Environment (ASE).[30] The BEEF-vdW exchange−correlation functional[31] was employed, as it has shown promising accuracy for the description of chemisorption as well as physisorption properties on transition metal surfaces.[31,32] Rh(111) and Rh(211) surfaces were modeled by periodic super cells containing four layers in the direction perpendicular to the surface separated by ∼18 Å of vacuum. The bottom two layers were kept fixed at their bulk positions, while the top two layers were allowed to relax. The Rh(111) slab was modeled using a 5 × 5 unit cell. The Rh(211) stepped surface consists of three-atoms columns comprising Rh(111)-type terraces, separated by one atom high Rh(100)-structure steps; this model is labeled as [3(111) × (100)] in step notation. For this study we considered a unit cell consisting of two terraces and five atoms in the direction running along the terraces (6 × 5 atoms per unit cell surface). That way, the Rh(111) and Rh(211) unit cells expose 25 and 30 surface Rh atoms, respectively. The gamma-centered k-point meshes were 2 × 2 × 1.

The Rh $5s^1$, $4d^8$, the C $2s^2$, $2p^2$, the O $2s^2$, $2p^4$, and the H $1s^1$ electrons were treated as valence electrons, while the remaining electrons were kept frozen as core states within the representation of the projector-augmented wave (PAW) method.[33] The Kohn−Sham equations were solved self-consistently using a plane-wave basis with a cutoff energy of 500 eV and a first order Methfessel−Paxton smearing of 0.2 eV. Structural relaxations were performed according to the Hellmann−Feynman scheme with the tolerance for the maximum force acting on each atom being 0.02 eV/Å. All calculations were performed using dipole-correction by adding a compensating electric field as implemented in the VASP code. Adsorption energies on Rh(111) and Rh(211) surfaces were defined as follows:

$$\Delta E_{ads} = E[\text{molecule/Rh\_surf}] - (E[\text{molecule}] + E[\text{Rh\_surf}]) \quad (1)$$

where E[molecule/Rh_surf] is the total energy of a system corresponding to a molecule adsorbed on Rh(111) or Rh(211) surface, E[molecule] is the total energy of the molecule in vacuum, and E[Rh_surf] is the total energy of the corresponding free Rh(111) or Rh(211) surface.

The nudged elastic band (NEB) method[34] has been applied to locate all transition states. This method was followed by the climbing-image NEB (CI-NEB)[35] method to locate the transition states more precisely. We checked the configurations of all transition states by calculating the vibrational frequencies. For each transition-state we obtained one imaginary vibrational frequency confirming a first order saddle point. Vibrational frequencies analysis was performed with a normal-mode analysis by using a finite-difference approximation of the Hessian matrix, as implemented in VASP, with a step size of 0.04 Å for the numerical differentiation.

The sensitivity of the DFT results with respect to the GGA approach has been obtained through an ensemble of exchange-correlation functionals representing the known computational error of the BEEF-vdW functional for chemisorption energies as reported elsewhere.[36]

2.2. Microkinetic Modeling. The kinetic model was solved using CatMap, an open source microkinetic modeling module.[37,38] The model uses the mean-field approximation, and the rate equations are solved following a steady-state approximation, iterating through a root-finding algorithm. Convergence was reached when the coverages of all intermediates change with less than 10^{-50}. Two different sites have been considered: one for all adsorbates (free sites on Rh surfaces) and one site for hydrogen. In this approach, hydrogen is adsorbed on a special "hydrogen reservoir" site,[39] not competing with other adsorbates for a free site. The degree of rate control (DRC) analysis was performed as implemented in CatMap using the approach outlined in ref 40.

3. RESULTS

Herein we report density functional theory calculations of the hydrodeoxygenation (HDO) of phenol and cyclohexanol on Rh(111) and Rh(211) surfaces (see Figure 1). The first section deals with the HDO of phenol. This is followed by an

DOI: 10.1021/acs.jpcc.6b02970
J. Phys. Chem. C 2016, 120, 18529−18537

investigation of cyclohexanol HDO. The last section shows the outcome of microkinetic modeling of the processes on the two different surfaces.

3.1. Phenol Hydrodeoxygenation on Rh(111) and Rh(211). Direct deoxygenation (DDO) is considered a promising route for the production of aromatics from lignin precursors.[18,20,41] In the DDO of phenolic compounds, their C−O bond is cleaved without prior hydrogenation of the aromatic ring thus producing aromatic compounds directly. Here, we use phenol as a representative of this class of molecules. We assume the following pathway for the production of benzene from phenol:

$$C_6H_5OH(g) + * \leftrightarrow C_6H_5OH* \quad (2)$$

$$C_6H_5OH* + * \leftrightarrow C_6H_5* + OH* \quad (3)$$

$$H_2(g) + 2*^h \leftrightarrow 2H*^h \quad (4)$$

$$C_6H_5* + H*^h \leftrightarrow C_6H_6* + *^h \quad (5)$$

$$H*^h + OH* \leftrightarrow H_2O(g) + * + *^h \quad (6)$$

$$C_6H_6* \leftrightarrow C_6H_6(g) + * \quad (7)$$

where * denotes an empty site on the surface and $*^h$ represents an empty "hydrogen reservoir" site. In this reaction network, phenol adsorbs on the surface (step 2), followed by cleavage of its C−O bond to produce adsorbed benzyl (C_6H_5*) (step 3). This benzyl is hydrogenated by surface bound hydrogen to produce benzene (step 5). Desorption of hydroxyl as water (step 6) and benzene (step 7) closes the catalytic cycle.

We start by investigating the adsorption of phenol on Rh(111). The obtained geometry is similar to previous theoretical studies[26] with phenol being adsorbed in a flat position about 2.07 Å above the surface. The calculated adsorption energy of phenol at 1/25 ML is −1.64 eV (see Figure 2a,b for the structure). Here the coverage is defined as the number of adsorbates per surface Rh atoms. Note that due to the size of phenol, approximately six atoms of the (111) surface are covered by one molecule of phenol. Our calculated adsorption energy for phenol on Rh(211) is −1.67 eV at 1/30 ML coverage (see Figure 2c,d for the structure), thus only slightly larger than the value found for Rh(111). Coverages on Rh(211) surfaces are defined as the number of adsorbates divided by the total number of surface atoms of the Rh(211) slab. The BEEF-vdW value for benzene adsorption is calculated to −1.67 and −1.55 eV for Rh(111) and Rh(211), respectively (see Figure S8 for the structures). Adsorption energy of phenol and benzene seems to be similar, and we also note that there is no apparent structure sensitivity for the two surfaces investigated here.

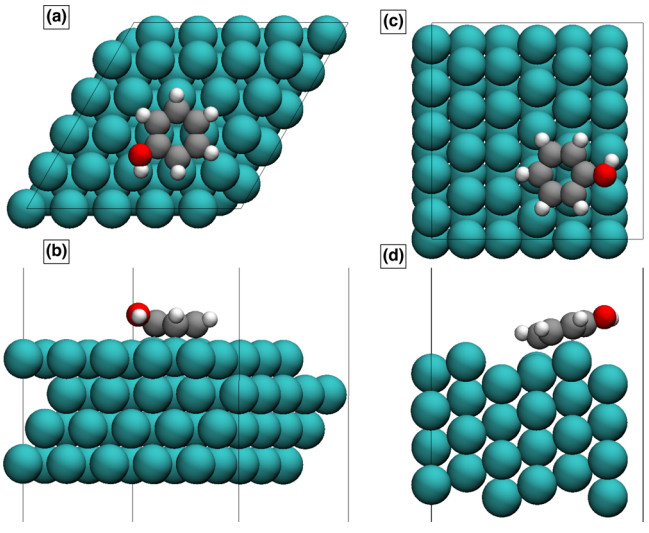

Figure 2. Most stable structures of phenol adsorbed on the Rh(111) and Rh(211) slabs. Top (a) and side (b) views of phenol/Rh(111). Top (c) and side (d) views of the phenol/Rh(211).

Table 1 compares our calculated results with those from other theoretical studies. There are several studies on the adsorption of benzene on Rh(111), and we note that the value obtained with the BEEF-vdW functional is generally within the reported range from −1.48 to −2.79 eV.[42−44] We note that this range is rather large, reflecting the difficulty of obtaining reliable benzene adsorption energies on transition metal surfaces owing to the problematic description of its aromaticity within density functional theory.[42] Generally it can be seen that using functionals that account for dispersion forces bind benzene strongest. Phenol adsorption on Rh(111) and Rh(211) has been calculated earlier using the PW91 functional.[26] While the calculated phenol adsorption on Rh(211) of −1.79 eV is close to the value obtained in this study (−1.67 eV), the calculated phenol adsorption on Rh(111) is much larger being −2.79 eV compared to our value of −1.64 eV. We note that the structure of the adsorbed phenol in that study is rather similar to the one calculated here, so that the large discrepancy in adsorption energies must be related to the differences in functionals. It has been shown previously that PW91 tends to systematically overestimate binding energies of smaller adsorbates, whereas BEEF-vdW does not show significant mean-signed errors for adsorption energies.[32] Whether the differences are due to this general trend, however, is difficult to quantify. It has been shown that BEEF-vdW tends to underestimate benzene adsorption energies on Pt(111) surfaces.[32] Given the similarity between Rh and Pt, a similar trend could be expected, which

Table 1. Comparison of Benzene and Phenol Adsorption Energies on Rh(111) and Rh(211) Surfaces

molecule	surface	functional	coverage (ML)[a]	ΔE_{ads} (eV)[b]	ref
phenol	Rh(111)	BEEF-vdW	1/25	−1.64	this work
	Rh(211)	BEEF-vdW	1/30	−1.67	this work
	Rh(111)	PW91	1/25	−2.79	26
	Rh(211)	PW91	1/25	−1.79	26
benzene	Rh(111)	BEEF-vdW	1/25	−1.67	this work
	Rh(211)	BEEF-vdW	1/30	−1.55	this work
	Rh(111)	PBE	1/9	−1.48	42
	Rh(111)	PBE + vdW	1/9	−2.79	43
	Rh(111)	PBE + vdW^{surf}	1/9	−2.52	42
	Rh(111)	optB88-vdW	1/9	−2.27	42
	Rh(111)	PW91	1/9	−1.53	44

[a]These coverages are defined as the number of gas molecules per metal surface atom. [b]These energies of adsorption are nonzero-point energy (ZPE) corrected. ZPE are reported in Table S7 of the SI.

DOI: 10.1021/acs.jpcc.6b02970
J. Phys. Chem. C 2016, 120, 18529−18537

would explain why adsorption values with BEEF-vdW are at the lower end of the various data shown in Table 1.

We will now discuss the DDO pathway on Rh(111) where phenol is hydrodeoxygenated to benzene and water. The free energy diagram of this reaction is shown in Figure 3 (purple lines). Adsorption of phenol (see Figure 3a) is followed by cleavage of the C−O bond yielding C_6H_5* and OH* (see Figure 3b,c for the structures of the C_6H_5−OH* transition state and the C_6H_5* intermediate, respectively). An activation barrier of 1.69 eV (ΔG = 1.55 eV) accompanies this reaction step. The next step constitutes the dissociative adsorption of H_2, which is calculated to −0.60 eV. This value compares well with the experimental value of −0.73 eV.[32,45] The free energy of hydrogen adsorption at 550 K is slightly endothermic by 0.07 eV (see Figure 3). The reaction of hydrogen with C_6H_5* yielding adsorbed benzene (C_6H_6*) is calculated to have a reaction barrier of 0.5 eV (ΔG = 0.47 eV) (see Figure 3d,e for the structures of the C_6H_5−H* transition state and C_6H_6*). The barrier for the formation of H_2O from H*^{h} and OH* is slightly higher being 0.87 eV (ΔG = 0.78 eV) (see Figure 3). Desorption of benzene, which is calculated to have an adsorption free energy of −1.67 eV, is closing the catalytic cycle. Note that this step is still endothermic by 0.56 eV at a reaction temperature of 550 K. Judging from the reaction free energy diagram in Figure 3 it seems that possible obstacles for the conversion of phenol to benzene on Rh(111) are the large activation barrier for C−O cleavage and the strong adsorption of both phenol and benzene, possibly leading to poisoning of the surface.

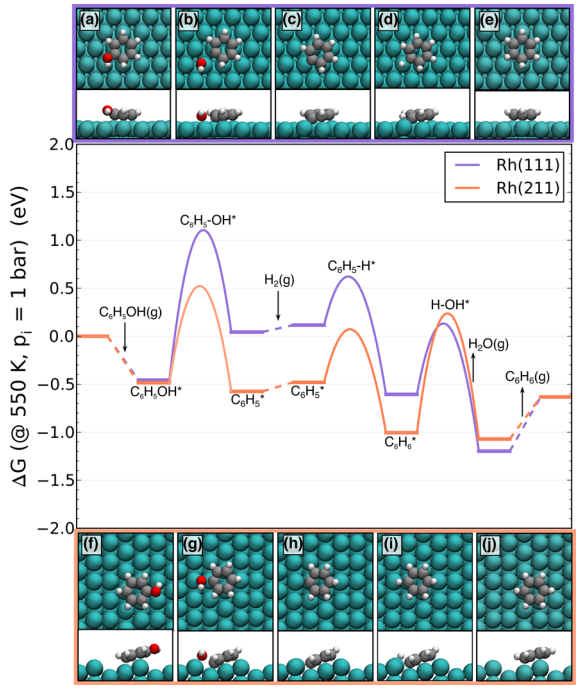

Figure 3. Gibbs free energy reaction pathways of the hydrodeoxygenation of phenol to benzene on Rh(111) (purple line) and Rh(211) (orange line) at a temperature of 550 K and standard pressures of all gas-phase species. Structures of intermediates and transition states C_6H_5OH*, C_6H_5−OH*, C_6H_5*, C_6H_5−H*, and C_6H_6* adsorbed on Rh(111) and Rh(211) can be seen in subfigures (a) to (e) and (f) to (j), respectively.

The free energy diagram of phenol conversion to benzene on the Rh(211) surface is also shown in Figure 3 (orange lines). In Figure 3f we show the most stable structure for phenol adsorption on the Rh(211) surface, while Figure 3g shows the transition state for C−O bond break with the OH* being opposite to its original position in Figure 3f. This implies a 180° rotation around an axis perpendicular to the surface passing through the center of the aromatic ring, which leads to the configuration of higher energy (ΔE_{ads} = −1.35) that can be seen in Figure S3d of the SI. Phenol then can cleave its C−O bond leading to a stable configuration as shown in Figure 3h. The barrier for C−O bond cleavage is 1.14 eV (ΔG = 1.01 eV) and thus significantly lower on this surface (see Figure 3h for the structure of the C_6H_5* intermediate). The same is true for the chemisorption energies of C_6H_5* and OH* relative to gas-phase phenol. These species bind 0.08 and 0.54 eV stronger on the Rh(211) than on the Rh(111), respectively. Hydrogen adsorption on Rh(211) is similar to Rh(111) and the barrier for the reaction C_6H_5* + H*^{h} → C_6H_6* + *^{h} is nearly the same as on Rh(111), 0.57 eV (ΔG = 0.53 eV) (see Figure 3i,j for the structures of the C_6H_5−H* transition state and the C_6H_6* intermediate, respectively). Interestingly, removal of OH* as H_2O is accompanied by a high reaction barrier of 1.33 eV (ΔG = 1.24 eV) on Rh(211). The final step is the desorption of benzene, which is slightly less endothermic than on Rh(111) being 0.44 eV at 550 K.

In order to analyze the difference in reactivity between Rh(111) and Rh(211) in more detail we performed a microkinetic analysis of the DDO of phenol to benzene, and Figure 4 shows the turnover frequency (TOF) of this reaction for Rh(111) (purple line) and Rh(211) (orange line) as a function of temperature at 10 bar total pressure and phenol:H_2 molar ratio of 1:9 at 1% conversion. DDO of phenol to benzene has a negligible TOF of 3.9 × 10^{-6} site^{-1} s^{-1} at a temperature of 550 K indicating that this reaction will hardly take place on Rh(111) under these reaction conditions. The Rh(211) surface, however, is calculated to have a TOF of 2.2 × 10^{-1} site^{-1} s^{-1}, an increase of 5 orders of magnitude compared to Rh(111). Rh(211) thus presents a feasible site for the DDO

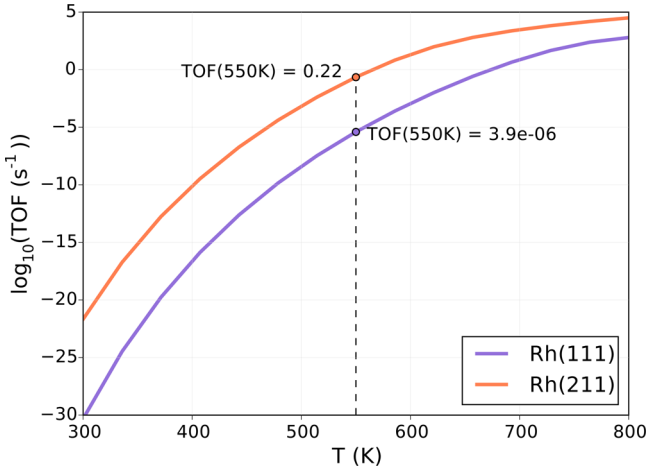

Figure 4. Logarithm of the turnover frequency (TOF) as a function of temperature for the conversion of phenol to benzene on Rh(111) (purple line) and Rh(211) (orange line) as calculated from a microkinetic model and the data shown in Figure 3. Reaction conditions are p = 10 bar, C_6H_5OH/H_2 ratio = 1:9, and differential reaction conditions (1% conversion).

DOI: 10.1021/acs.jpcc.6b02970
J. Phys. Chem. C 2016, 120, 18529−18537

of phenol to benzene. Figure 5 shows the coverages of all intermediates as a function of temperature, with the reaction

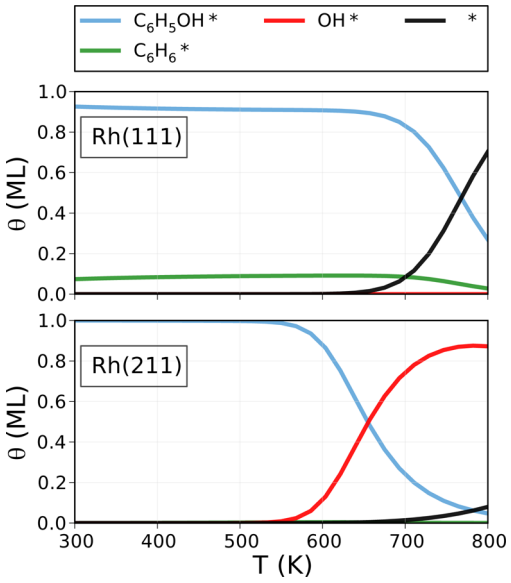

Figure 5. Coverages of intermediates as a function of temperature for the conversion of phenol to benzene on Rh(111) (top) and on Rh(211) (bottom) as obtained from the steady state solution to the microkinetic model. Reaction conditions are p = 10 bar, C_6H_5OH/H_2 ratio = 1:9, and differential reaction conditions (1% conversion). Coverages of C_6H_5* are below 10^{-4} ML for the whole temperature range considered (see Figure S11 of the SI for a logarithmic plot of all coverages). Hydrogen is adsorbed on a hydrogen reservoir site, the coverage of which is shown in the SI.

conditions being the same as those in Figure 4 (see Table S8 of the SI for coverages of all intermediates at a temperature of 550 K). It can be seen that both surfaces are covered by close to 1 monolayer (ML) of adsorbates with Rh(111) having a coverage of both phenol (0.91 ML) and benzene (0.09 ML) and Rh(211) being covered by 0.99 ML of phenol under steady state conditions and temperatures up to ∼700 and ∼600 K, respectively. We highlight that this kinetic model is normalized to yield a total coverage of all intermediates other than hydrogen equal to 1. While this model uses the energies computed above as an input, we stress that the coverages are defined differently as in Table 1, in an attempt to simplify the model and the solution to the model. Note that hydrogen is adsorbed on a different lattice and hence does not compete with the adsorption of other intermediates (see Methods section).

We also performed an analysis of rate-determining steps using Campbell's degree of rate control (DRC),[40] the results of which are summarized in Table 2. As expected from the free energy diagram in Figure 3, the transition state with the highest DRC is the splitting of the C−O bond in phenol. Moreover, the analysis shows that adsorbed phenol is the intermediate with the highest DRC for both surfaces. An improved catalyst would hence have a lower lying transition state for C−O bond splitting while at the same time adsorbing phenol (and benzene) more weakly.

3.2. Cyclohexanol Hydrodeoxygenation on Rh(111) and Rh(211). Cyclohexanol is the product of the full hydrogenation of the aromatic ring of phenol. Phenol can hence be converted to alkanes such as cyclohexane and *n*-

Table 2. Degrees of Rate Control of All Intermediates and Transition States for the Conversion of Phenol to Benzene on Rh(111) and Rh(211) As Obtained from the DRC Analysis[a]

	degree of rate control X_i	
species	Rh(111)	Rh(211)
Intermediates		
H*[h]	0.00	−0.01
C_6H_5OH*	−1.82	−1.96
C_6H_5*	0.00	0.00
C_6H_6*	−0.18	−0.01
OH*	0.00	−0.02
Transition States		
C_6H_5−OH*	1.00	0.98
C_6H_5−H*	0.00	0.00
H−OH*	0.00	0.02

[a]Reaction conditions are p = 10 bar, T = 550 K, C_6H_5OH/H_2 ratio = 1:9, and differential reaction conditions (1% conversion).

hexane via the cyclohexanol intermediate (see Figure 1b). While we do not investigate the mechanism of the hydrogenation of phenol to cyclohexanol herein we note that hydrogenation barriers for phenol are generally small on transition metal surfaces as they are found to be within the range 0.76 to 1.35 eV.[23,24,27,46] Our focus here is to evaluate the hydrodeoxygenation of cyclohexanol to cyclohexane on both Rh(111) and Rh(211) and compare the reactivity of cyclohexanol to that found for phenol. There are various routes for the conversion of cyclohexanol to cyclohexane.[27] The first pathway considers C−OH bond breaking as shown above for phenol. Other possibilities are hydrogenation−dehydration (HYD) routes where cyclohexanol would be dehydrated to cyclohexene and water followed by the hydrogenation to cyclohexane as well as other hydrogen assisted routes. Theoretical studies on Fe(110) and Pd(111) surfaces indicate that direct cleavage of the C−OH bond is faster than the HYD as well as other routes.[27] In addition, this contribution intends to compare the cleavage of the C−O bonds in phenol and cyclohexanol. We therefore restrict this study to the direct cleavage of the C−OH bond in cyclohexanol. The resulting pathway looks similar to that established for phenol above and consists of the following reaction steps:

$$C_6H_{11}OH(g) + * \leftrightarrow C_6H_{11}OH* \quad (8)$$

$$C_6H_{11}OH* + * \leftrightarrow C_6H_{11}* + OH* \quad (9)$$

$$H_2(g) + 2*^h \leftrightarrow 2H*^h \quad (10)$$

$$C_6H_{11}* + H*^h \leftrightarrow C_6H_{12}* + *^h \quad (11)$$

$$H*^h + OH* \leftrightarrow H_2O(g) + * + *^h \quad (12)$$

$$C_6H_{12}* \leftrightarrow C_6H_{12}(g) + * \quad (13)$$

note that reaction steps 10 and 12 are identical to 4 and 6 above. The first step of the catalytic cycle consists of the adsorption of cyclohexanol (step 8), which is calculated to be −0.66 and −0.91 eV on Rh(111) (see Figure 6a) and Rh(211) (see Figure 6f), respectively (also see Figure S6 for structures). Due to the large entropic loss upon adsorption, however, this step is uphill in free energy at a reaction temperature of 550 K for both surfaces (ΔG = 0.44 eV and ΔG = 0.19 eV for

DOI: 10.1021/acs.jpcc.6b02970
J. Phys. Chem. C 2016, 120, 18529−18537

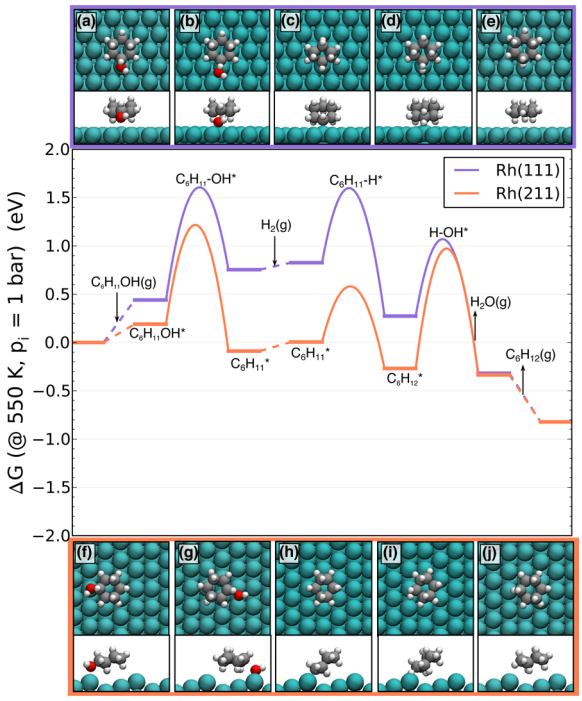

Figure 6. Gibbs free energy reaction pathways of the hydrodeoxygenation of cyclohexanol to cyclohexane on Rh(111) (purple line) and Rh(211) (orange line) at a temperature of 550 K and standard pressures of all gas-phase species. Structures of intermediates and transition states $C_6H_{11}OH^*$, $C_6H_{11}–OH^*$, $C_6H_{11}^*$, $C_6H_{11}–H^*$, and $C_6H_{12}^*$ adsorbed on Rh(111) and Rh(211) can be seen in subfigures (a) to (e) and (f) to (j), respectively.

Rh(111) and Rh(211), respectively) (see Figure 6). Cleavage of the C−O bond (step 9) is associated with barriers of 1.30 (ΔG = 1.16 eV) and 1.16 eV (ΔG = 1.02 eV) for Rh(111) (see Figure 6b) and Rh(211) (see Figure 6g), respectively. The structures of $C_6H_{11}^*$ intermediates on both Rh(111) and Rh(211) surfaces can be observed in Figure 6c,h, respectively. The next step consists of the addition of a hydrogen atom to the cyclohexyl intermediate ($C_6H_{11}^*$) (step 11) with barriers of 0.79 (ΔG = 0.78 eV) and 0.61 eV (ΔG = 0.57 eV) on Rh(111) (see Figure 6d) and Rh(211) (see Figure 6i) surfaces, respectively. As discussed for the DDO of phenol, removal of OH* from the surface is more difficult for Rh(211) compared to Rh(111). The last step of the catalytic cycle consists of desorption of cyclohexane (step 13). The adsorption energy of cyclohexane is −0.46 and −0.47 eV for Rh(111) (see Figure 6e) and Rh(211) (see Figure 6j), respectively (also see Figure S9 for structures), so that the desorption becomes exothermic at 550 K (ΔG = −0.50 eV and ΔG = −0.49 eV, respectively).

The difference in reactivity between Rh(111) and Rh(211) is analyzed in more detail using a microkinetic analysis of the HDO of cyclohexanol to cyclohexane. This is shown in Figure 7 where the TOF is plotted as a function of temperature for Rh(111) (purple line) and Rh(211) (orange line). Similar to the DDO of phenol, the activity of Rh(211) is higher than that of Rh(111). In this case the TOF differ by about 3 orders of magnitude with Rh(211) having a TOF of 1.5×10^{1} site^{-1} s^{-1} and Rh(111) a TOF of 2.5×10^{-2} site^{-1} s^{-1}. It thus seems that both Rh(211) and to some extent Rh(111) are able to convert cyclohexanol to cyclohexane at 550 K. Figure 8 shows the coverages of all intermediates as a function of temperature, with the reaction conditions being the same as in Figure 7. Due to

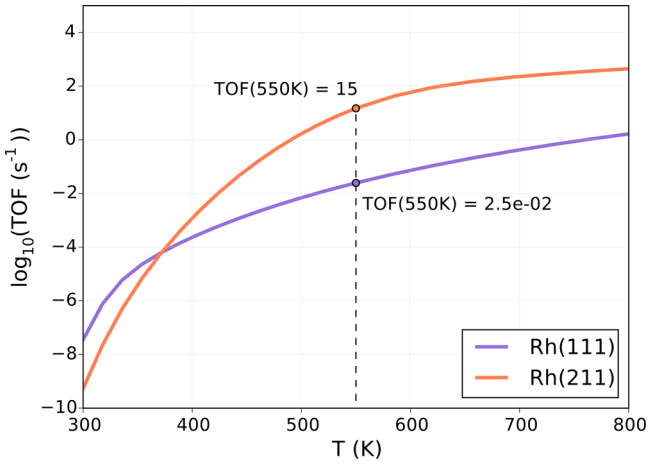

Figure 7. Logarithm of the turnover frequency (TOF) as a function of temperature for the conversion of cyclohexanol to cyclohexane on Rh(111) (purple line) and Rh(211) (orange line) as calculated from a microkinetic model and the data shown in Figure 6. Reaction conditions are p = 10 bar, $C_6H_{11}OH/H_2$ ratio = 1:9, and differential reaction conditions (1% conversion).

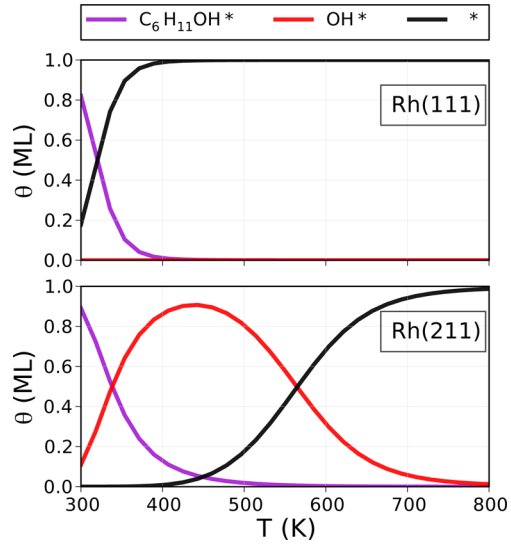

Figure 8. Coverages of intermediates as a function of temperature for the conversion of cyclohexanol to cyclohexane on Rh(111) (top) and Rh(211) (bottom) as obtained from the steady state solution of the microkinetic model. Reaction conditions are p = 10 bar, $C_6H_{11}OH/H_2$ ratio = 1:9, and differential reaction conditions (1% conversion). Coverages of $C_6H_{11}^*$ and $C_6H_{12}^*$ are below 10^{-4} ML for the whole temperature range considered (see Figure S12 of the SI for a logarithmic plot of all coverages). Hydrogen is adsorbed on a hydrogen reservoir site the coverage of which is shown in the SI.

the weak binding of cyclohexanol and cyclohexane there are no appreciable coverages of these intermediates and Rh(111) is essentially free of any adsorbates (with the coverage of free sites, θ^*, being close to 1). On Rh(211), however, adsorption of OH* is still strong and we calculate an OH* coverage of 0.58 ML at a reaction temperature of 550 K at steady state (see also Table S9 of the SI).

Rate-controlling steps are analyzed using the DRC method, the results of which are summarized in Table 3. The DRC of the C−O bond splitting is 1 in the case of Rh(111). For Rh(211), however, the DRC of this step is only 0.27 with the hydrogenation of adsorbed OH* to yield water having a DRC

DOI: 10.1021/acs.jpcc.6b02970
J. Phys. Chem. C 2016, 120, 18529−18537

Table 3. Degrees of Rate Control of All Intermediates and Transition States for the Conversion of Cyclohexanol to Cyclohexane on Rh(111) and Rh(211) As Obtained from the DRC Analysis[a]

	degree of rate control X_i	
species	Rh(111)	Rh(211)
Intermediates		
H*	0.00	−0.38
$C_6H_{11}OH$*	0.00	−0.01
C_6H_{11}*	0.00	0.00
C_6H_{12}*	0.00	0.00
OH*	0.00	−0.74
Transition States		
C_6H_{11}−OH*	1.00	0.27
C_6H_{11}−H*	0.00	0.00
H−OH*	0.00	0.73

[a]Reaction conditions are p = 10 bar, T = 550 K, $C_6H_{11}OH/H_2$ ratio = 1:9, and differential reaction conditions (1% conversion).

of 0.73. In addition, while no intermediates have any DRC for Rh(111) the OH* intermediate has a DRC of −0.74 on Rh(211), again indicating its strong binding to the Rh(211) site that is also evident from its high coverage under reaction conditions. The model employed here does only consider the reaction of cyclohexanol to cyclohexane without any aromatics in the reaction mixture. However, under phenol HDO conditions there would be phenol and perhaps also benzene present, which would heavily cover the surface due to their strong adsorption energies (see also above). The rates calculated here do therefore represent an upper bound of cyclohexanol HDO in the limit where there are negligible gas-phase concentrations of phenol and benzene.

4. DISCUSSION

Comparing C−O bond splitting over Rh(111) and Rh(211) we find that the latter surface is more active for both types of C−O bond splitting considered. As might be expected, C−O bond splitting of adsorbed phenol is more difficult than for cyclohexanol. While Rh(211) is calculated to be able to split the C−O bond in both, phenol and cyclohexanol, with appreciable rates, Rh(111) is unable to convert phenol. In an attempt to identify factors governing the structure−activity relationships of C−O bond splitting we turn our attention to the correlation between the transition and final state energy of the C−O bond breaking reactions. The resulting transition-state scaling relation[47] is shown in Figure 9. Apart from the data herein, we also included similar data on various transition metal surfaces calculated with other functionals such as the PW91 and PBE functional. While it seems counterintuitive to compare the results of different functionals, especially when these functionals obtain very different results regarding adsorption energies (see Table 1), we stress here that our focus lies on the correlation between the transition state energy (ΔE_{TS}) and the final state energy (ΔE_{FS}) rather than their absolute values. As evident from Figure 9, there is a strong correlation between ΔE_{TS} and ΔE_{FS} for all data points considered. We performed a sensitivity analysis of our calculated values using the BEEF-vdW ensemble of exchange correlation functionals,[31,36] and the results are shown as principle component ellipses in Figure 9. While the error of our calculated results is estimated to ±0.3 eV, we note that there is a strong correlation between ΔE_{TS} and ΔE_{FS} indicative of a general scaling that is independent of the

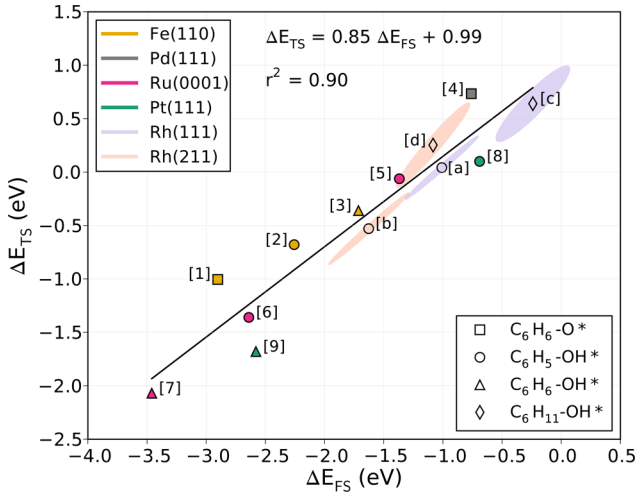

Figure 9. Correlation between transition state energies (ΔE_{TS}) and final state energies (ΔE_{FS}) for C−O bond breaking in C_6H_6−O* (squares), C_6H_5−OH* (circles), C_6H_6−OH* (triangles), and C_6H_{11}−OH* (routes) on Fe(110) (yellow), Pd(111) (gray), Ru(0001) (magenta), Pt(111) (green), Rh(111) (purple), and Rh(211) (orange). All energies are taken relative to the gas-phase molecules (either phenol or cyclohexanol). In the case of C_6H_6−OH* this corresponds to gas-phase phenol and 1/2 gas phase H_2. Data points a−d are taken from this study, while 1−9 are taken from the literature. Ellipsoid axes for a−d are determined from a principal component analysis of the Bayesian error estimation ensembles.[36] Data points are [a] C_6H_5−OH* on Rh(111) calculated with BEEF-vdW; [b] C_6H_5−OH* on Rh(211) calculated with BEEF-vdW; [c] C_6H_{11}−OH* on Rh(111) calculated with BEEF-vdW; [d] C_6H_{11}−OH* on Rh(211) calculated with BEEF-vdW; [1] C_6H_6−O* on Fe(110) calculated with PW91;[27] [2] C_6H_5−OH* on Fe(110) calculated with PW91;[27] [3] C_6H_6−OH* on Fe(110) calculated with PW91;[27] [4] C_6H_6−O* on Pd(111) calculated with PW91;[27] [5] C_6H_5−OH* on Ru(0001) calculated with PBE;[22] [6] C_6H_5−OH* on Ru(0001) calculated with PBE-D3;[23] [7] C_6H_6−OH* on Ru(0001) calculated with PBE-D3;[23] [8] C_6H_5−OH* on Pt(111) calculated with PBE-D3;[24] [9] C_6H_6−OH* on Pt(111) calculated with PBE-D3.[24] Note that the extra hydrogen of C_6H_6−OH* is located on the *ortho* carbon atom for data points [7] and [9] and that the carbon atom is attached to the OH* for data point [3].

functional used. This is also evident when comparing our results to data obtained with the PBE and PW91 functional (see Figure 9) that generally follows the same transition state scaling relation. Interestingly, C−O bond breaking for both surfaces, Rh(111) and Rh(211) lies roughly on the same scaling line, and the rate increase observed between Rh(111) and Rh(211) for the two reactions considered here (see Figures 4 and 7) is solely due to a shift along the scaling line toward stronger binding.

We investigated the HDO of phenol and cyclohexanol using 5 × 5 and 6 × 5 surfaces to present the active sites of Rh(111) and Rh(211), respectively. We thus assume a moderate coverage with distances between, e.g., two phenol molecules on Rh(111) being 8 Å. We note, however, that there may be adsorbate−adsorbate interactions at higher coverages that may decrease the binding energy of phenol as well as other intermediates and transition states. This coverage dependence would ultimately also have to be included in the microkinetic model in order to draw a more realistic picture of the reactions investigated here. We also point out that the description of adsorption energies of phenol and benzene with DFT is difficult, as also reflected by the wide range of values reported in

DOI: 10.1021/acs.jpcc.6b02970
J. Phys. Chem. C 2016, 120, 18529−18537

the literature (see Table 1). It is therefore conceivable that the error might be substantial and higher than our estimation using the Bayesian error estimation ensemble suggests (see Figure 9). One way to target these uncertainties is to include correction schemes to systematically account for the errors associated with DFT.[48]

5. CONCLUSIONS

We established trends in the C−O bond breaking of phenol and cyclohexanol and investigated the structure sensitivity of these reactions. We found that C−O bond breaking is easier in cyclohexanol owing to the hydrogenation of the aromatic ring before cleavage, which weakens the C−O bond energy. Furthermore, the stepped Rh(211) surface is more active than Rh(111). The increase in activity, however, is solely due to the increased binding of the final state after cleavage and both surfaces are subject to the same transition-state scaling. Our analysis indicates that rhodium catalysts should be able to break the C−O bonds in both, phenol and cyclohexanol, with an appreciable rate. If benzene is the desired product, one would have to find ways to suppress hydrogenation of the aromatic ring in phenol and/or benzene. From a thermodynamic point of view, this could be obtained through a low hydrogen pressure and a high temperature. We established a relationship between transition state energies of C−O bond cleavage and the final state. This descriptor-based approach for the analysis of C−O cleavage trends presents a first important step toward the computational design of HDO catalysts.

■ ASSOCIATED CONTENT

Supporting Information

The Supporting Information is available free of charge on the ACS Publications website at DOI: 10.1021/acs.jpcc.6b02970.

Additional details on the DFT and thermochemistry calculations (PDF)

■ AUTHOR INFORMATION

Corresponding Author

*E-mail: felix.studt@kit.edu. Phone: +49 721-608-28663.

Notes

The authors declare no competing financial interest.

■ ACKNOWLEDGMENTS

The work is funded by Innovation Fund Denmark under the H2CAP−Hydrogen assisted catalytic biomass pyrolysis for green fuels project (no. 1305-00015B), which is gratefully acknowledged. We gratefully acknowledge the support from the U.S. Department of Energy, Office of Basic Energy Sciences to the SUNCAT Center for Interface Science and Catalysis. The authors would like to thank Jens K. Nørskov for fruitful discussions.

■ REFERENCES

(1) Murray, J.; King, D. Oil's tipping point has passed. *Nature* **2012**, *481*, 433−435.

(2) Kerr, R. A. An Oil Gusher in the Offing, but Will It Be Enough? *Science* **2012**, *338*, 1139.

(3) Mortensen, P. M.; Grunwaldt, J.-D.; Jensen, P. A.; Knudsen, K. G.; Jensen, A. D. A review of catalytic upgrading of bio-oil to engine fuels. *Appl. Catal., A* **2011**, *407*, 1.

(4) Choudhary, T. V.; Phillips, C. B. Renewable fuels via catalytic hydrodeoxygenation. *Appl. Catal., A* **2011**, *397*, 1.

(5) Venderbosch, R. H.; Prins, W. Fast pyrolysis technology development. *Biofuels, Bioprod. Biorefin.* **2010**, *4*, 178.

(6) Wildschut, J.; Melián-Cabrera, I.; Heeres, H. J. Catalyst Studies on the Hydrotreatment of Fast Pyrolysis Oil. *Appl. Catal., B* **2010**, *99*, 298−306.

(7) Zhao, C.; He, J.; Lemonidou, A. A.; Li, X.; Lercher, J. A. Aqueous-Phase Hydrodeoxygenation of Bio-Derived Phenols to Cycloalkanes. *J. Catal.* **2011**, *280*, 8−16.

(8) Boullosa-Eiras, S.; Lødeng, R.; Bergem, H.; Stöcker, M.; Hannevold, L.; Blekkan, E. A. Catalytic Hydrodeoxygenation (HDO) of Phenol over Supported Molybdenum Carbide, Nitride, Phosphide and Oxide Catalysts. *Catal. Today* **2014**, *223*, 44−53.

(9) Xu, H.; Wang, K.; Zhang, H.; Hao, L.; Xu, J.; Liu, Z. Ionic Liquid Modified Montmorillonite-Supported Ru Nanoparticles: Highly Efficient Heterogeneous Catalysts for the Hydrodeoxygenation of Phenolic Compounds to Cycloalkanes. *Catal. Sci. Technol.* **2014**, *4*, 2658.

(10) Zhao, C.; Kasakov, S.; He, J.; Lercher, J. A. Comparison of Kinetics, Activity and Stability of Ni/HZSM-5 and Ni/Al_2O_3-HZSM-5 for Phenol Hydrodeoxygenation. *J. Catal.* **2012**, *296*, 12−23.

(11) Zhao, C.; Camaioni, D. M.; Lercher, J. A. Selective Catalytic Hydroalkylation and Deoxygenation of Substituted Phenols to Bicycloalkanes. *J. Catal.* **2012**, *288*, 92−103.

(12) Yoosuk, B.; Tumnantong, D.; Prasassarakich, P. Amorphous Unsupported Ni−Mo Sulfide Prepared by One Step Hydrothermal Method for Phenol Hydrodeoxygenation. *Fuel* **2012**, *91*, 246−252.

(13) Ohta, H.; Kobayashi, H.; Hara, K.; Fukuoka, A. Hydrodeoxygenation of Phenols as Lignin Models under Acid-Free Conditions with Carbon-Supported Platinum Catalysts. *Chem. Commun.* **2011**, *47*, 12209.

(14) Ryymin, E.-M.; Honkela, M. L.; Viljava, T.-R.; Krause, A. O. I. Competitive Reactions and Mechanisms in the Simultaneous HDO of Phenol and Methyl Heptanoate over Sulphided NiMo/γ-Al_2O_3. *Appl. Catal., A* **2010**, *389*, 114−121.

(15) Hong, D.-Y.; Miller, S. J.; Agrawal, P. K.; Jones, C. W. Hydrodeoxygenation and Coupling of Aqueous Phenolics over Bifunctional Zeolite-Supported Metal Catalysts. *Chem. Commun.* **2010**, *46*, 1038.

(16) Yakovlev, V. A.; Khromova, S. A.; Sherstyuk, O. V.; Dundich, V. O.; Ermakov, D. Y.; Novopashina, V. M.; Lebedev, M. Y.; Bulavchenko, O.; Parmon, V. N. Development of New Catalytic Systems for Upgraded Bio-Fuels Production from Bio-Crude-Oil and Biodiesel. *Catal. Today* **2009**, *144*, 362−366.

(17) Yang, Y. Q.; Tye, C. T.; Smith, K. J. Influence of MoS_2 Catalyst Morphology on the Hydrodeoxygenation of Phenols. *Catal. Commun.* **2008**, *9*, 1364−1368.

(18) Popov, A.; Kondratieva, E.; Mariey, L.; Goupil, J. M.; El Fallah, J.; Gilson, J.-P.; Travert, A.; Maugé, F. Bio-Oil Hydrodeoxygenation: Adsorption of Phenolic Compounds on Sulfided (Co)Mo Catalysts. *J. Catal.* **2013**, *297*, 176−186.

(19) Zhang, W.; Chen, J.; Liu, R.; Wang, S.; Chen, L.; Li, K. Hydrodeoxygenation of Lignin-Derived Phenolic Monomers and Dimers to Alkane Fuels over Bifunctional Zeolite-Supported Metal Catalysts. *ACS Sustainable Chem. Eng.* **2014**, *2*, 683−691.

(20) Romero, Y.; Richard, F.; Brunet, S. Hydrodeoxygenation of 2-Ethylphenol as a Model Compound of Bio-Crude over Sulfided Mo-Based Catalysts: Promoting Effect and Reaction Mechanism. *Appl. Catal., B* **2010**, *98*, 213−223.

(21) Mortensen, P. M.; Grunwaldt, J.-D.; Jensen, P. A.; Jensen, A. D. Screening of Catalysts for Hydrodeoxygenation of Phenol as a Model Compound for Bio-Oil. *ACS Catal.* **2013**, *3*, 1774−1785.

(22) Chiu, C.; Genest, A.; Borgna, A.; Rösch, N. Hydrodeoxygenation of Guaiacol over Ru(0001): A DFT Study. *ACS Catal.* **2014**, *4*, 4178−4188.

(23) Lu, J.; Heyden, A. Theoretical Investigation of the Reaction Mechanism of the Hydrodeoxygenation of Guaiacol over a Ru(0001) Model Surface. *J. Catal.* **2015**, *321*, 39−50.

DOI: 10.1021/acs.jpcc.6b02970
J. Phys. Chem. C 2016, 120, 18529−18537

(24) Lu, J.; Behtash, S.; Mamun, O.; Heyden, A. Theoretical Investigation of the Reaction Mechanism of the Guaiacol Hydrogenation over a Pt(111) Catalyst. *ACS Catal.* **2015**, *5*, 2423−2435.
(25) Yu, W.; Xiong, K.; Ji, N.; Porosoff, M. D.; Chen, J. G. Theoretical and Experimental Studies of the Adsorption Geometry and Reaction Pathways of Furfural over FeNi Bimetallic Model Surfaces and Supported Catalysts. *J. Catal.* **2014**, *317*, 253−262.
(26) Honkela, M. L.; Björk, J.; Persson, M. Computational Study of the Adsorption and Dissociation of Phenol on Pt and Rh Surfaces. *Phys. Chem. Chem. Phys.* **2012**, *14*, 5849.
(27) Hensley, A. J. R.; Wang, Y.; McEwen, J.-S. Phenol Deoxygenation Mechanisms on Fe(110) and Pd(111). *ACS Catal.* **2015**, *5*, 523.
(28) Kresse, G.; Furthmüller, J. Efficiency of Ab-Initio Total Energy Calculations for Metals and Semiconductors Using a Plane-Wave Basis Set. *Comput. Mater. Sci.* **1996**, *6*, 15−50.
(29) Kresse, G.; Hafner, J. Ab Initio Molecular Dynamics for Liquid Metals. *Phys. Rev. B: Condens. Matter Mater. Phys.* **1993**, *47*, 558−561.
(30) Bahn, S. R.; Jacobsen, K. W. An Object-Oriented Scripting Interface to a Legacy Electronic Structure Code. *Comput. Sci. Eng.* **2002**, *4*, 56−66.
(31) Wellendorff, J.; Lundgaard, K. T.; Møgelhøj, A.; Petzold, V.; Landis, D. D.; Nørskov, J. K.; Bligaard, T.; Jacobsen, K. W. Density Functionals for Surface Science: Exchange-Correlation Model Development with Bayesian Error Estimation. *Phys. Rev. B: Condens. Matter Mater. Phys.* **2012**, *85*, 235149.
(32) Wellendorff, J.; Silbaugh, T. L.; Garcia-Pintos, D.; Nørskov, J. K.; Bligaard, T.; Studt, F.; Campbell, C. T. A Benchmark database for adsorption bond energies to transition metal surfaces and comparison to selected DFT functionals. *Surf. Sci.* **2015**, *640*, 36.
(33) Kresse, G.; Joubert, D. From Ultrasoft Pseudopotentials to the Projector Augmented-Wave Method. *Phys. Rev. B: Condens. Matter Mater. Phys.* **1999**, *59*, 1758−1775.
(34) Jónsson, H.; Mills, G.; Jacobsen, K. W. Nudged Elastic Band Method for Finding Minimum Energy Paths of Transitions. In *Classical and Quantum Dynamics in Condensed Phase Simulations*; Berne, B. J., Ciccotti, G., Coker, D. F., Eds.; World Scientific, 1998.
(35) Henkelman, G.; Uberuaga, B. P.; Jónsson, H. A Climbing Image Nudged Elastic Band Method for Finding Saddle Points and Minimum Energy Paths. *J. Chem. Phys.* **2000**, *113*, 9901−9904.
(36) Medford, A. J.; Wellendorff, J.; Vojvodic, A.; Studt, F.; Abild-Pedersen, F.; Jacobsen, K. W.; Bligaard, T.; Nørskov, J. K. Assessing the reliability of calculated catalytic ammonia synthesis rates. *Science* **2014**, *345*, 197.
(37) Medford, A. J.; Shi, C.; Hoffmann, M. J.; Lausche, A. C.; Fitzgibbon, S. R.; Bligaard, T.; Nørskov, J. K. CatMAP: A Software Package for Descriptor-Based Microkinetic Mapping of Catalytic Trends. *Catal. Lett.* **2015**, *145*, 794−807.
(38) CATMAP GitHub Repository. https://github.com/ajmedford/catmap (accessed Aug 20, 2015).
(39) Lausche, A. C.; Medford, A. J.; Khan, T. S.; Xu, Y.; Bligaard, T.; Abild-Pedersen, F.; Nørskov, J. K.; Studt, F. On the effect of coverage-dependent adsorbate-adsorbate interactions for CO methanation on transition metal surfaces. *J. Catal.* **2013**, *307*, 275.
(40) Stegelmann, C.; Andreasen, A.; Campbell, C. T. Degree of Rate Control: How Much the Energies of Intermediates and Transition States Control Rates. *J. Am. Chem. Soc.* **2009**, *131*, 8077.
(41) Wang, W.; Zhang, K.; Li, L.; Wu, K.; Liu, P.; Yang, Y. Synthesis of Highly Active Co−Mo−S Unsupported Catalysts by a One-Step Hydrothermal Method for *p* -Cresol Hydrodeoxygenation. *Ind. Eng. Chem. Res.* **2014**, *53*, 19001−19009.
(42) Liu, W.; Carrasco, J.; Santra, B.; Michaelides, A.; Scheffler, M.; Tkatchenko, A. Benzene Adsorbed on Metals: Concerted Effect of Covalency and van Der Waals Bonding. *Phys. Rev. B: Condens. Matter Mater. Phys.* **2012**, *86*, 245405.
(43) Liu, W.; Ruiz, V. G.; Zhang, G.-X.; Santra, B.; Ren, X.; Scheffler, M.; Tkatchenko, A. Structure and Energetics of Benzene Adsorbed on Transition-Metal Surfaces: Density-Functional Theory with van Der Waals Interactions Including Collective Substrate Response. *New J. Phys.* **2013**, *15*, 053046.
(44) Morin, C.; Simon, D.; Sautet, P. Chemisorption of Benzene on Pt(111), Pd(111), and Rh(111) Metal Surfaces: A Structural and Vibrational Comparison from First Principles. *J. Phys. Chem. B* **2004**, *108*, 5653−5665.
(45) Yates, J. T., Jr.; Thiel, P. A.; Weinberg, W. H. The Chemisorption of Hydrogen on Rh(111). *Surf. Sci.* **1979**, *84*, 427−439.
(46) Yoon, Y.; Rousseau, R.; Weber, R. S.; Mei, D.; Lercher, J. A. First-Principles Study of Phenol Hydrogenation on Pt and Ni Catalysts in Aqueous Phase. *J. Am. Chem. Soc.* **2014**, *136*, 10287−10298.
(47) Wang, S.; Temel, B.; Shen, J.; Jones, G.; Grabow, L. C.; Studt, F.; Bligaard, T.; Abild-Pedersen, F.; Christensen, C. H.; Nørskov, J. K. Universal Brønsted-Evans-Polanyi Relations for C-C, C-O, C-N, N-O, N-N, and O-O Dissociation Reactions. *Catal. Lett.* **2011**, *141*, 370.
(48) Christensen, R.; Hansen, H. A.; Vegge, T. Identifying systematic DFT errors in catalytic reactions. *Catal. Sci. Technol.* **2015**, *5*, 4946.

DOI: 10.1021/acs.jpcc.6b02970
J. Phys. Chem. C 2016, 120, 18529−18537